Original Article

Diagnostic performance of CT-derived resting distal to aortic pressure ratio (resting Pd/Pa) *vs.* CT-derived fractional flow reserve (CT-FFR) in coronary lesion severity assessment

Quan Li[1#], Yang Zhang[1#], Chunliang Wang[2,3], Shiming Dong[4], Yijin Mao[3], Yida Tang[5], Yong Zeng[1]

[1]Center for Coronary Artery Disease, Division of Cardiology Beijing Anzhen Hospital, Capital Medical University, Beijing, China; [2]Departement of Biomedical Engineering and Health Systems, KTH - Royal Institute of Technology, Stockholm, Sweden; [3]Shenzhen Escope Tech Inc., China; [4]Department of Cardiology, Changzheng Hospital, Second Military Medical University, Shanghai, China; [5]Department of Cardiovascular Medicine, Peking University Third Hospital, Beijing, China

Contributions: (I) Conception and design: Q Li, S Dong, Y Mao; (II) Administrative support: Y Tang, Y Zeng; (III) Provision of study materials or patients: Q Li, Y Zhang; (IV) Collection and assembly of data: All authors; (V) Data analysis and interpretation: All authors; (VI) Manuscript writing: All authors; (VII) Final approval of manuscript: All authors.

[#]These authors contributed equally to this work.

Correspondence to: Yong Zeng, MD. Center for Coronary Artery Disease, Division of Cardiology Beijing Anzhen Hospital, Capital Medical University, Beijing 100029, China. Email: yzeng_anzhen@163.com; Yida Tang, MD. Department of Cardiovascular Medicine, Peking University Third Hospital, Beijing 100191, China. Email: tang_yida@163.com.

Background: Computed tomography-derived fractional flow reserve (CT-FFR) has emerged as a promising non-invasive substitute for fractional flow reserve (FFR) measurement. Normally, CT-FFR providing functional significance of coronary artery disease (CAD) by using a simplified total coronary resistance index (TCRI) model. Yet the error or discrepancy caused by this simplified model remains unclear.

Methods: A total of 20 consecutive patients with suspected CAD who underwent CTA and invasive FFR measurement were retrospectively analyzed. CT-FFR and CT-$(Pd/Pa)_{rest}$ values derived from the coronary CTA images. The diagnostic performance of CT-FFR and CT-$(Pd/Pa)_{rest}$ were evaluated on a per-vessel level using C statistics with invasive FFR<0.80 as the reference standard.

Results: Of the 25 vessels eventually analyzed, the prevalence of functionally significant CAD were 64%. The Youden index of the ROC curve indicated that the best cutoff value of invasive resting Pd/Pa was 0.945 for identifying functionally significant lesions. Sensitivity, specificity, negative predictive value, positive predictive value and accuracy were 85%, 91%, 92%, 83% and 88% for CT-$(Pd/Pa)_{rest}$ and 85%, 58% 69%, 78% and 72% for CT-FFR. Area under the receiver-operating characteristic curve (AUC) to detect functionally significant stenoses of CT-$(Pd/Pa)_{rest}$ and CT-FFR were 0.87 and 0.90.

Conclusions: In this study, the results suggest CT-derived resting Pd/Pa has a potential advantage over CT-FFR in triaging patients for revascularization.

Keywords: Fractional flow reserve (FFR); computational fluid dynamics; coronary CT angiography; pressure ratio

Submitted Jul 23, 2021. Accepted for publication Sep 03, 2021.
doi: 10.21037/atm-21-4325
View this article at: https://dx.doi.org/10.21037/atm-21-4325

Introduction

In the early 1990s, researchers including Pijls and De Bruyne established the experimental basis for determining the relative maximum flow from pressure measurement (Pd/Pa) during hyperemia and claimed this measurement (now called fractional flow reserve, FFR) might have a potential clinical application for assessing the functional severity of stenosis during percutaneous transluminal coronary

angioplasty (1). In this concept, as part of the maximum value that can be expected in the absence of stenosis, the maximum myocardial perfusion that can be achieved in the presence of stenosis can be assessed by measuring coronary artery pressure. The concept of FFR is based on the assumption that there is an approximate linear correlation between coronary perfusion pressure and flow during the maximum expansion of coronary artery bed. Theoretically, pressure measurements at the distal and proximal segments of coronary stenosis can be used to estimate the ratio of coronary flow in stenosis to that in the absence of stenosis (2). Since the introduction of FFR, many investigations have been conducted and demonstrated its excellent performance in both diagnosis and prognosis (3), and it is now adopted as a first-line diagnostic tool with the highest level of clinical evidence (Class-IA-recommendation) in the European Society of Cardiology/European Association for Cardio-Thoracic Surgery (ECS/EACTS) guidelines of 2018 on myocardial revascularization (4), with an adjusted cut-off value (5).

However, the clinical adoption of FFR faces some practical obstacles due to its requirement of vasodilator administration, which cannot be tolerated by certain groups of patients (4). Due to the high consistency with FFR, the resting distal coronary artery pressure aortic pressure (Pd/PA) ratio (calculated as the average non-hyperemic transstenotic pressure ratio throughout the cardiac cycle) is proposed as a simpler indicator than FFR to estimate the severity of stenosis (6). In 2013, Jeremias (7) conducted the first coronary physiology study (The RESOLVE Study) that employed a core laboratory for the analysis of hyperemic and resting pressure derived indices of stenosis severity and found both resting Pd/Pa and iFR could achieve equivalent accuracy of ~80% compared to FFR as the reference standard. Lee (8) studied the correlation between resting Pd/Pa and iFR based on 1,024 vessels of 435 patients and concluded that resting Pd/Pa showed similar associations with the risk of MACE as iFR. Kobayashi also carried out a multi-center clinical trial on 763 patients and validated the agreement of resting Pd/Pa with iFR, while other studies (9,10) have also suggested resting Pd/Pa is a more practical and safer vasodilator-free physiological index compared to FFR.

To reduce the cost and risk caused by the invasive measurement of these physiological indexes, computational fluid engineers have developed methods to compute the FFR value via numerical simulation of the hemodynamics using 3D anatomical models created from computed tomography angiography (CTA). Fractional flow reserve derived from coronary CTA (CT-FFR) is a noninvasive physiological test used to evaluate the flow restriction caused by coronary artery stenosis. It has good diagnostic accuracy and good correlation with invasive FFR (11). In the recent ADVANCE registry, the prognostic value of CT-FFR has also been fully affirmed (12). Nevertheless, some critical flaws in the methodology of CT-FFR must be addressed as they could undermine the reliability of its results. A recent systematic review conducted by Cook (13) has shown a discrepancy between the simulated CT-FFR and measured FFR around of the gray zone of FFR, and the diagnostic performance of CT-FFR has been demonstrated to be rather poor within the critical gray zone. Recent investigations (14-17) have suggested the main reasons for the disappointing diagnostic accuracy of CT-FFR in the gray zone might be the result of: (I) an inaccurate baseline level of distributed coronary flow in each branch; (II) uncertainty related to the reduction in peripheral resistance due to vasodilation administration; and (III) the 3D vessel segmentation error seen around severe stenosis, which is crucial for the CT-FFR prediction. To address these problems, Taylor *et al.* (18) estimated the baseline flow for each branch under resting conditions via a simplified model related to the radius of distal vessels, and to mimic the state of maximum hyperemia, a circuit-like model and so-called total coronary resistance index (TCRI) model was introduced. In essence, the TCRI model is an empirical equation of estimating the reduction of the peripheral resistance by simply assuming heart rate is an ultimate reflection of all reasons affecting the index (19). Müller *et al.* have found that the reduction of peripheral resistance is the dominant factor affecting CT-FFR accuracy via a comprehensive sensitivity analysis of all possible factors (20). However, it was also found that the TCRI model could only be accurately determined by the calibration of coronary flow reserve ahead, which is the ratio of total coronary flow at maximum hyperemia at rest.

With the purpose of removing the error induced by TCRI, we hypothesize that CT-derived resting Pd/Pa could potentially perform better for the "gray-zone" cases than CT-FFR. With respect to computational fluid dynamics, accuracy of any blood flow related simulation result, including derived index such as resting Pd/Pa and FFR, is very sensitive to the provided coronary blood flow (CBF) which is very difficult to obtain. However, all essential information of CBF is indeed implicitly embodied in the CT image for each specific patient. Therefore, this study was to investigate the accuracy of the TCRI based CT-

FFR and CT derived resting Pd/PA for the identification of functionally relevant coronary artery disease (CAD). On the other hand, considering the good diagnostic performance of resting Pd/Pa and its advantage of no vasodilator requirement, we believe it is very meaningful to investigate the relationship between resting Pd/Pa and CT-$(Pd/Pa)_{rest}$ under resting conditions. We present the following article in accordance with the STARD reporting checklist (available at https://dx.doi.org/10.21037/atm-21-4325).

Methods

Study population and clinical measurements

The analysis involved 25 vessels from 20 patients suspected of CAD who presented between February 2013 and March 2017 to the Capital Medical University Affiliated Anzhen Hospital, and the calculation of CT-$(Pd/Pa)_{rest}$, CT-FFR, invasive resting Pd/Pa, and FFR indices. The inclusion criteria were patients who underwent coronary CTA by CT scanners with 64-row detectors or more and invasive coronary angiography (ICA), and the corresponding FFR measurements were conducted within the next 30 days after coronary CTA. The exclusion criteria were: (I) major peri-procedure adverse cardiac events (myocardial infarction, cardiac death, or emergent revascularization); (II) complicated congenital heart diseases; (III) previous coronary artery bypass surgery or stenting; (IV) installed pacemaker; (V) artificial heart valves; (VI) bifurcation stenosis; (VII) chronic total occlusion; (VIII) non-diagnostic quality of CTA data; (IX) body mass index (BMI) ≥35; (X) prior myocardial infarction; or (XI) an unqualified pressure curve for resting Pd/Pa or FFR analysis.

All procedures performed in this study involving human participants were in accordance with the Declaration of Helsinki (as revised in 2013). The study was approved by Beijing Anzhen Hospital committee board of ethics (No.: 2020091X) and informed consent was taken from all the patients. No author had access to information that could identify individual participants during or after data collection. The authors are solely responsible for the design and conduct of this study, all study analyses, the drafting and editing of the paper, and its final content. For the CT image acquisition, multidetector scanners with more than 64-row detector from three leading manufactures (Somatom Definition, Siemens, Forchheim, Germany; Aquilion One, Toshiba, Otawara, Japan; Optima CT660, GE Healthcare, Milwaukee, WI) were used. CTA was performed in accordance with standard protocol (21), and prospective triggering was used for scan acquisitions. The core laboratory followed the quality standards as defined in guidelines (22). Oral beta-blockers were administered targeting a heart rate of <60 beats/min, and sublingual nitrates were administered to ensure coronary vasodilation. Data acquisition was performed with 100-kV tube voltage in patients weighing 70 kg and 120 kV in subjects weighing >70 kg.

For FFR and resting Pd/Pa measurement, two cardiologists, each with over 10 years' experience of CTA image analysis, performed invasive coronary angiography (ICA) using 6-7F guiding catheters without side holes by a radial or femoral approach. FFR and resting Pd/Pa were performed with a 0.014-inch PressureWire™, and the pressure sensor was positioned at least 30mm distal to the end of the stenosis. Before measurement, nitrates were used to control vasomotor tone and record the stable pressure wave. Resting Pd/Pa was first calculated as the mean pressure distal to the stenosis during the whole cardiac cycle, and FFR was then measured as the mean distal coronary pressure (Pd) divided by the mean aortic pressure (Pa) during maximal hyperemia. FFR was measured with the same coronary pressure guidewire at maximal hyperemia that was induced by adenosine triphosphate (ATP) administration. ATP was injected at 140 μg/kg/min for at least 2 minutes through a large forearm vein using an infusion pump until the heart rate began to increase while the Pd/Pa ratio remained steady. Pressure wire pullback was performed at each lesion segment for pressure drift check as shown in *Figure 1A*. If a Pd/Pa ratio <0.98 or >1.02 at the catheter tip was documented, the protocol mandated repeat assessment, while stenosis with an FFR value of <0.8 was considered as hemodynamically significant.

Numerical model and methodology

A senior researcher at an independent core laboratory blinded to the FFR and ICA results carried out CT-FFR and CT-$(Pd/Pa)_{rest}$ simulations. The calculation of CT-FFR and CT-$(Pd/Pa)_{rest}$ consisted of three major procedures as follows (*Figure 1B*): Step 1: the patient-specific coronary arterial trees were segmented by using a semi-automated software developed at KTH Royal Institute of Technology. For more details, the algorithm for the vessel segmentation was described in a previous paper (23), and its performance has been validated in previous studies (24). For each patient, a detailed 3D model was built to cover the entire coronary

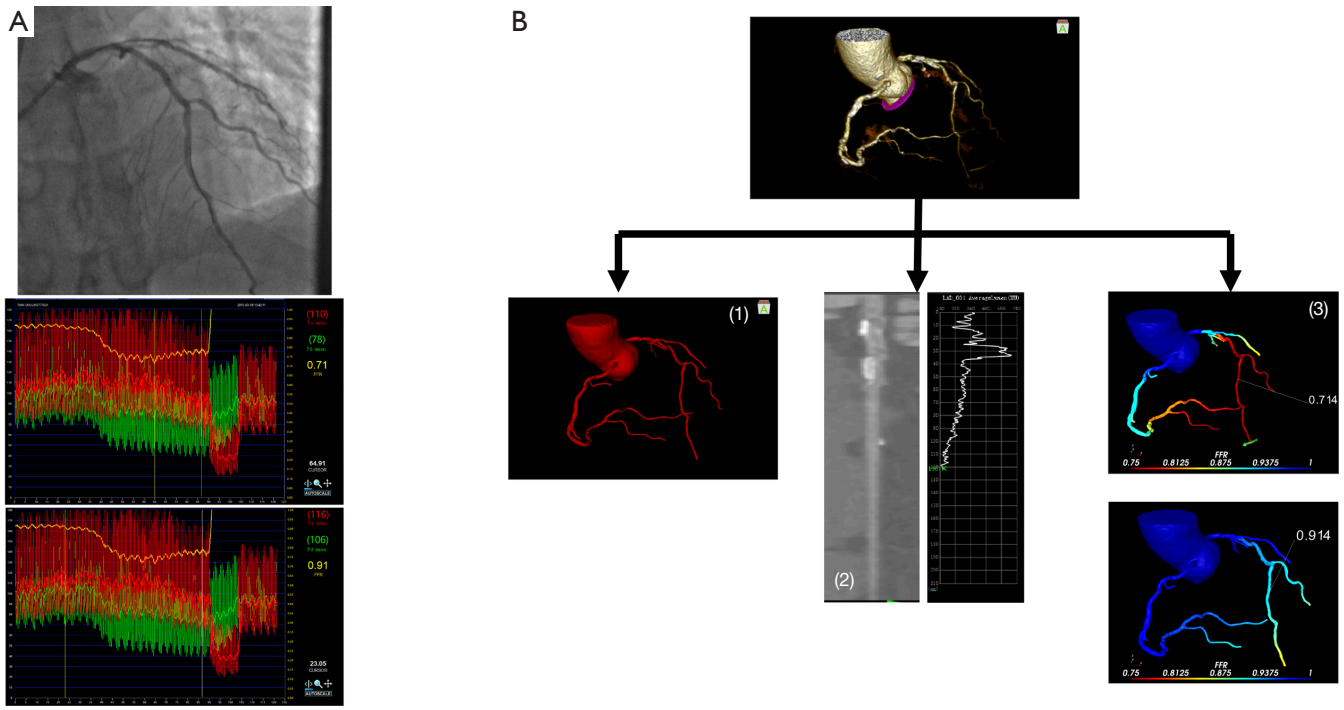

Figure 1 Schematic presentation of the CT-FFR and CT-$(Pd/Pa)_{rest}$ analysis. (A) Invasive FFR was measured 20 mm distal (white star) to the LAD stenosis of a 64 years old male patient. Invasive resting Pd/Pa was measured before vasodilator administration, while invasive FFR was measured following the standard procedures. (B) The three steps of CT-FFR and CT-$(Pd/Pa)_{rest}$ calculation procedures. CT-FFR, computed tomography angiography-derived fractional flow reserve. Step 1: a medical imaging tool whose performance was well validated at KTH (20,21) was applied to extract detailed coronary arterial trees with aorta included; Step 2: with respect to fluid dynamics, accuracy of blood flow related dynamics, including derived index such as resting Pd/Pa and FFR, is very sensitive to the provided coronary blood flow (CBF). Different from simplified but widely used models (16), this work has particularly calibrated the CBF for each interested branch via making full use of information implicitly embodied in the CT image for each specific patient. The detailed derivations of current approach can be found in (22) and its clinical evaluation is published in (23); Step 3: Once coronary tree and CBF are ready, the computational fluid dynamics simulation (OpenFOAM ver1912 OpenCFD Ltd.) was carried out for the calculation of CT-$(Pd/Pa)_{rest}$ and CT-FFR.

artery tree that included the main branches including the LAD, LCX, and RCA along with any discernible sub-branches. Human editing was performed wherever the automated segmentation failed to recover the exact vessel boundary. Step 2: for a reliable resting Pd/Pa and FFR simulation, it was necessary to quantify the coronary blood flow (CBF) for each branch. Other than some simplified models (18), an image derived model that could estimate the CBF for each branch using patient-specific information that was implicitly embodied in the CT image was adopted. The detailed derivations can be found in (25). Following a previous study, the transluminal contrast gradient (TCG) for each arterial vessel in CT images was generated due to the advection of the contrast bolus with time-varying contrast concentration that appeared at the coronary ostium. The TAG and coronary artery flow had an approximate relationship of Q-1/TAG, and the clinical evaluation of this model has already been studied in (26). Step 3: to mimic the real blood flow through the vessel, the open-source computational fluid dynamics (CFD) software, OpenFOAM ver1912 OpenCFD Ltd., was used to carry out the CFD simulation for the calculation of CT-$(Pd/Pa)_{rest}$ and CT-FFR.

Data management and physiological indices analysis

Patient baseline information was collected by clinicians from the cardiology department. Both resting Pd/Pa and invasive FFR were measured in the Catheter lab, and CT-$(Pd/Pa)_{rest}$ and CT-FFR calculations were conducted by a

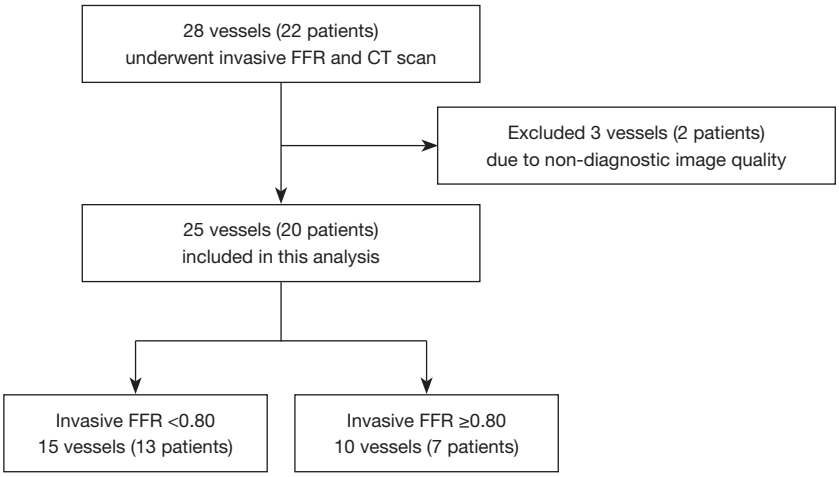

Figure 2 Flow diagram of the cohort selection. Study enrollments for 28 vessels of 22 patients, (three vessels of two patients were excluded). 25 vessels in 20 patients were included in the study.

trained operator from the core laboratory who was blinded to the invasive resting Pd/Pa and FFR result. Patient CTA images were provided by the radiology department to the core laboratory for the CT-FFR, CT-$(Pd/Pa)_{rest}$ calculation.

Statistical analysis

Categorical variables are presented by percentage and count, while continuous measurements were defined by their means and standard deviations. Mean value and quartile were used to represent the sample distribution. All data analyses were conducted on a per-vessel basis.

If the data satisfied the normal distribution, a parametric test was used, otherwise, a non-parametric test was employed. The accuracy, sensitivity, specificity, positive predictive value (PPV), and negative predictive value (NPV) of resting Pd/Pa, CT-FFR and CT-$(Pd/Pa)_{rest}$ were evaluated with FFR as a reference standard. The cut-off value for resting Pd/Pa was determined through the ROC curve with FFR as the ground truth, and the consistency was evaluated through Cohen's kappa. The systematic difference between CT-FFR and invasive FFR or between CT-$(Pd/Pa)_{rest}$ and resting Pd/Pa was represented through a Bland-Altman plot, which showed the portion of data out of maximal error.

The correlation between FFR and others, including CT-FFR, resting Pd/Pa, and CT-$(Pd/Pa)_{rest}$ respectively were represented by a correlation coefficient obtained through linear regression. P value less than 0.05 was considered as statistical significance. Statistics analysis in this study was conducted with the R version 4.0.0 (R Foundation for Statistical Computing, Vienna, Austria).

Results

Study protocol and patient characteristics

A total of 22 patients were enrolled and 20 were finally included in the analysis, as one was excluded due to non-diagnostic image quality as presented in *Figure 2*. We analyzed 25 vessels and all the statistical analysis was performed at the per-vessel level. Patient characteristics are presented in the *Table 1*, which shows the mean age of patients is 60.5 and 12 of 20 are males. As presented in *Table 2*, a total of seventeen left ascending (LAD) arteries, four left circumflex (LCX) arteries, three right coronary arteries (RCA) and one diagonal branch (Diag) were detected for possible lesions with stenosis level from 20–80%. Sixteen vessels (47%) were considered hemodynamically significant by an invasive FFR <0.80.

When comparing invasive resting Pd/Pa with FFR, there was a strong linear correlation (r=0.774, 95% CI: P<0.001) between resting Pd/Pa and FFR (*Figure 3*). The Youden index of the ROC curve indicated the best cutoff value of resting Pd/Pa was 0.945 corresponding to identify functionally significant lesions defined by FFR <0.80. With this cut-off value, the resting Pd/Pa results showed a total accuracy of 92%, sensitivity of 100%, specificity of 83%, PPV of 87%, and NPV of 100% as shown in the second column of. In addition, the C index (the area under the ROC curve) was 0.955 (95% CI: 0.87 to 1.00, P<0.001).

Diagnostic accuracy of CT-FFR compared to measured FFR

As shown in the *Figure 4*, CT-FFR also had an acceptable

Table 1 Baseline patient characteristics (n=20)

Characteristics	Values
Age, years	60.5±15.5
Male	12 [60]
Body mass index, kg/m^2	26.32±6.13
Diabetes mellitus	7 [35]
Hypertension	8 [40]
Hyperlipidemia	9 [45]
Current smoker	8 [40]
Family history of coronary artery disease	3 [15]
Clinical presentation	
Silent ischemia	2 [10]
Stable angina pectoris	3 [15]
Unstable angina pectoris	15 [75]

Values were mean ± SD or No. [%].

correlation with invasive FFR (r=0.731, P<0.001) and the area under the curve (AUC) was 0.888. A CT-FFR gray-zone was identified within the range of 0.70< CT-FFR <0.85, where most erroneous prediction occurred (see *Figure 5*). Further analysis on the systematic difference led to the result shown in the Bland-Altman plot in *Figure 6*, which demonstrates the mean difference between FFR and CT-FFR is 0.04, and the 95% limits of agreement is –0.07 to 0.15.

Diagnostic accuracy of CT-(Pd/Pa)$_{rest}$ compared to measured resting Pd/Pa

Figure 7 shows CT-(Pd/Pa)$_{rest}$ holds a stronger correlation with invasive resting Pd/Pa (r=0.824, P<0.001), and via the area under the curve (*Figure 7A*), that CT-(Pd/Pa)$_{rest}$ has almost no systematic difference and less variation against the invasive resting Pd/Pa value. It should be noted that the wrongly classified cases, as shown in *Figure 7B* and *Figure 8*, among which CT derived Pd/Pa is located between the range of (0.96, 0.98), could be in the possible "gray zone" of CT-(Pd/Pa)$_{rest}$. The mean difference resting Pd/Pa and CT-(Pd/Pa)$_{rest}$ was –0.01, and the 95% of limits of agreement were –0.06 to 0.04, as shown in *Figure 9*. All the above findings demonstrate better performance against CT-FFR. By comparing the diagnostic accuracy of CT-(Pd/Pa)$_{rest}$ and CT-FFR respectively, as shown in the third and fourth columns of *Table 3*, it can be seen the specificity is improved without sacrificing the sensitivity significantly. According to previous study (15), the higher specificity of CT-(Pd/Pa)$_{rest}$ was probably due to avoiding estimating the patient-specific CFR (or TCRI) that was in a large range when the stenosis was not severe.

Table 2 Patient and vessel characteristics according to coronary ICA, FFR, CT-FFR, and CT-(Pd/Pa)$_{rest}$ (n=25 vessels from 20 patients)

Characteristics	No. [%]
ICA and FFR characteristics	
Patients with coronary ICA maximum stenosis >70%	2 [10]
Patients with FFR <0.80	13 [65]
Vessels with FFR <0.80	15 [60]
Left anterior descending artery	12 [48]
Diagonal branch	1 [4]
Left circumflex artery	1 [4]
Right coronary artery	0 [0]
Patients with FFR <0.80 in >1 vessel	1 [4]
CT-FFR characteristics	
Patients with CT-FFR <0.80	14 [70]
Vessels with CT-FFR <0.80	16 [64]
Left anterior descending artery	11 [44]
Diagonal branch	1 [4]
Left circumflex artery	2 [8]
Right coronary artery	2 [8]
Patients with CR-FFR <0.80 in >1 vessel	1 [4]
CT-(Pd/Pa)rest characteristics	
Patients with CT-(Pd/Pa)$_{rest}$ <0.945	10 [50]
Vessels with CT-(Pd/Pa)$_{rest}$ <0.945	13 [65]
Left anterior descending artery	10 [50]
Diagonal branch	1 [4]
Left circumflex artery	2 [10]
Right coronary artery	0 [0]
Patients with CT-(Pd/Pa)$_{rest}$ <0.945 in >1 vessel	1 [4]

ICA, invasive coronary angiography; FFR, fractional flow reserve; CT-FFR, computed tomography angiography-derived fractional flow reserve.

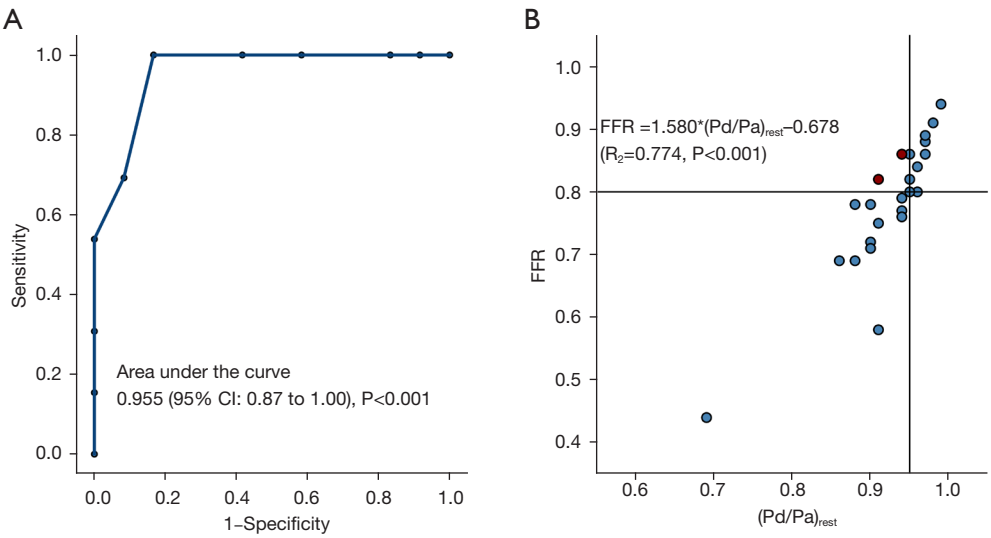

Figure 3 Diagnostic accuracy of resting Pd/Pa against FFR. (A) Area under the curve (AUC) of invasive resting Pd/Pa versus invasive FFR for the demonstration of ischemia (FFR <0.80) on a per-vessel basis; (B) linear correlation for invasive resting Pd/Pa and FFR. FFR <0.80 and resting Pd/Pa <0.945 were cut-offs for the diagnosis of ischemia, respectively. N=25 for per-vessel analysis. FFR, fractional flow reserve.

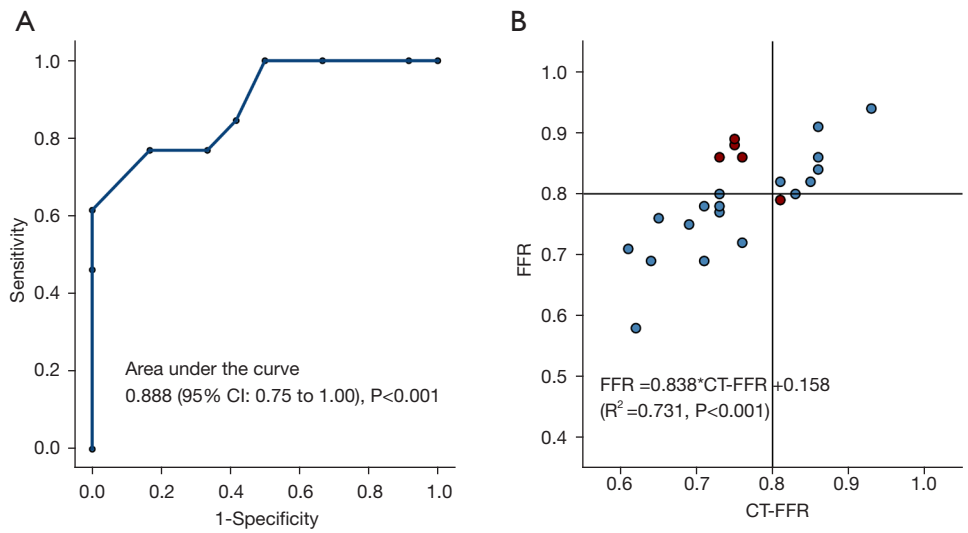

Figure 4 Diagnostic accuracy of resting CT-FFR against FFR. (A) Area under the curve (AUC) of CT-FFR versus invasive FFR for the demonstration of ischemia (FFR <0.80) on a per-vessel basis; (B) linear correlation for CT-FFR and FFR. A threshold value of 0.80 was used for the diagnosis of ischemia for both FFR and CT-FFR, while the total number of vessels is 25. CT-FFR, computed tomography angiography-derived fractional flow reserve.

Diagnostic accuracy of CT-(Pd/Pa)$_{rest}$ compared to measured FFR

We also inspected the possibility of using CT-(Pd/Pa)$_{rest}$ to substitute CT-FFR using invasive FFR as a reference standard, and CT-(Pd/Pa)$_{rest}$ <0.945 was identified as the cut-off threshold by the Youden index of the ROC curve associated with functionally significant lesions (invasive FFR <0.80). The AUC of CT-(Pd/Pa)$_{rest}$ was 0.907 (see *Figure 10*). With invasive FFR as ground truth, the diagnostic performance of CT-(Pd/Pa)$_{rest}$ showed a total accuracy of

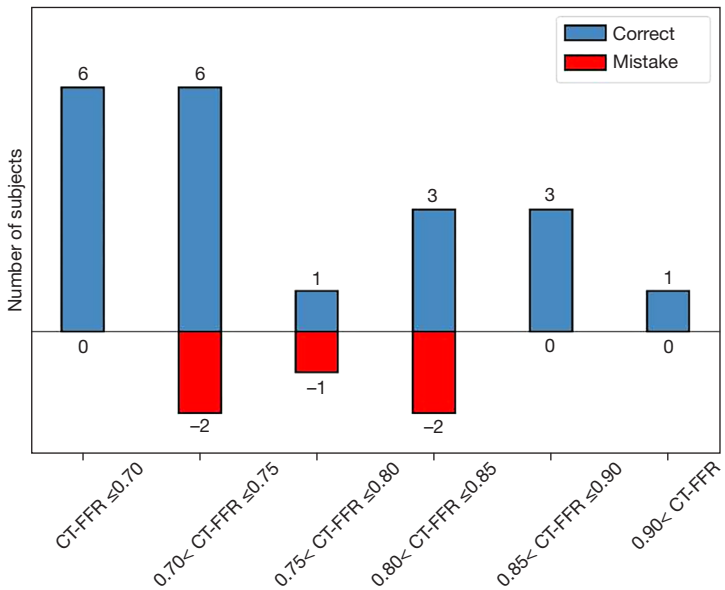

Figure 5 Diagnostic performance of CT-FFR among different ranges in correctly identifying lesions. The diagnostic "gray zone" was found between 0.70–0.85. CT-FFR, computed tomography angiography-derived fractional flow reserve.

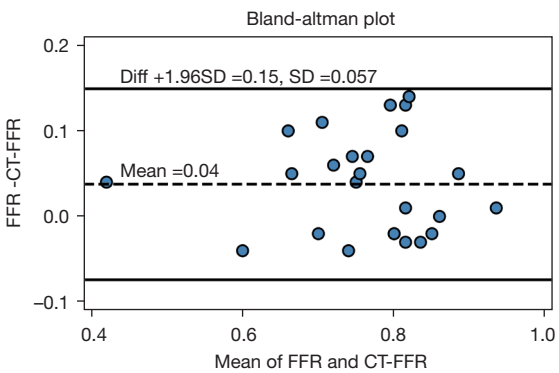

Figure 6 Bland-Altman plot of CT-FFR and invasive FFR on a per-vessel Basis. CT-FFR, computed tomography angiography-derived fractional flow reserve

88%, sensitivity of 85%, specificity of 91%, PPV of 92% and NPV of 83% (see *Table 3*).

Discussion

In this study, the cut-off value of 0.945 for resting Pd/Pa was determined by comparing it to the invasive FFR values, which is in good agreement with previous studies (27,28), and suggests the clinical application of resting Pd/Pa could be a good candidate index for early screening before performing FFR measurement. One study has shown a hybrid strategy of iFR-FFR could improve the classification accuracy to 94.7%, while 61% patients were diagnosed without the administration of a vasodilator through performing FFR only for those lesions within an iFR-gray zone of 0.86–0.93 (29). A few investigators have borrowed similar ideas and suggested the gray zone could be 0.90–0.93 for all non-hyperemic translesional pressure ratios (NHPRs), such as resting Pd/Pa (30). While the hybrid strategy of NHPR-FFR itself still requires more evidence to support its validity in actual clinical performance, it shows great prospect in completely eliminating adenosine use.

Encouraged by the promising results achieved with invasive resting Pd/Pa, we also put forward a noninvasive method to calculate resting Pd/Pa with computational fluid dynamics simulation solely based on non-invasive coronary CTA. Good correlation was found between CT-$(Pd/Pa)_{rest}$ and both resting Pd/Pa (R^2=0.824) and FFR (R^2=0.69) which was comparable to that of CT-FFR over FFR (R^2=0.731). Taking FFR <0.80 as a reference, the diagnostic performance of CT-$(Pd/Pa)_{rest}$ was satisfactory, with sensitivity of 0.85, specificity of 0.91, PPV of 0.92, and NPV of 0.83, whereas the performance of CT-FFR was inferior, with sensitivity of 0.85, specificity of 0.58, PPV of 0.69, and NPV of 0.78. In comparison to CT-FFR, which inevitably introduces errors using a TCRI model of predicting resistance under hyperemia (18), CT-(Pd/Pa)

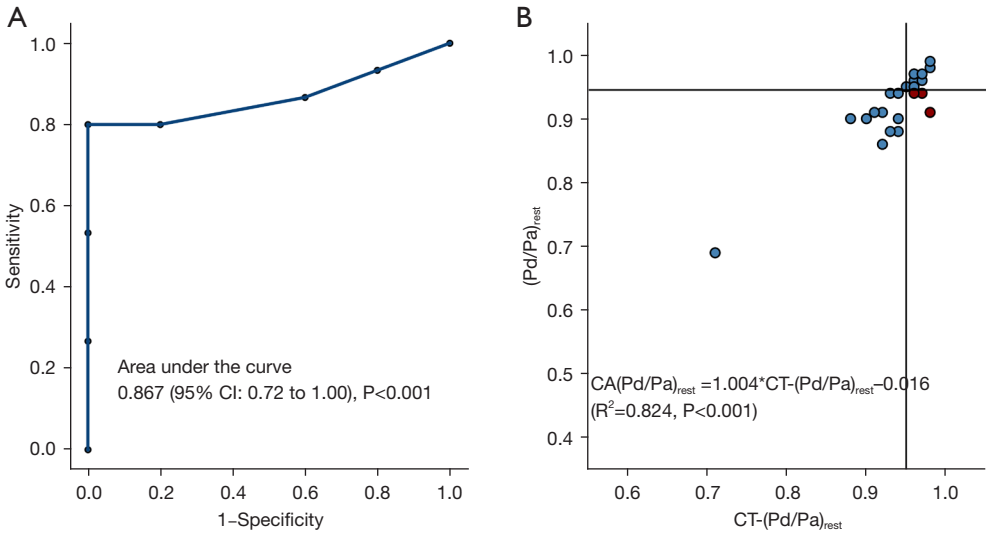

Figure 7 Diagnostic accuracy of resting CT-(Pd/Pa)$_{rest}$ against invasive resting Pd/Pa. (A) Area under the curve (AUC) of CT-(Pd/Pa)$_{rest}$ versus invasive resting Pd/Pa for demonstration of ischemia (resting Pd/Pa <0.945) on a per-vessel basis; (B) Linear correlation for CT-(Pd/Pa)$_{rest}$ and invasive resting Pd/Pa. Invasive resting Pd/Pa/ CT-(Pd/Pa)$_{rest}$ <0.945 were cut-offs for the diagnosis of ischemia. N=25 for per-vessel analysis.

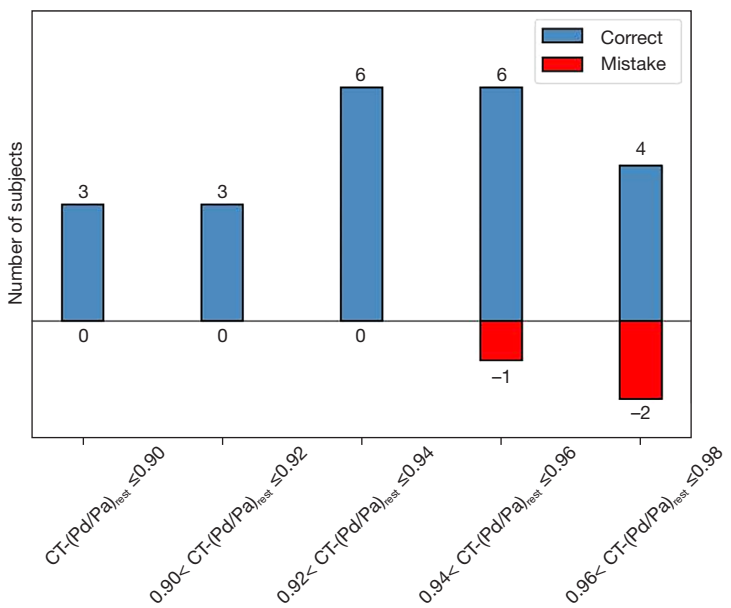

Figure 8 Diagnostic performance of CT-(Pd/Pa)rest among different ranges in correctly identifying lesions. The diagnostic "gray zone" was found between 0.96–0.98.

$_{rest}$ computation raised no such concerns. This confirms the poor specificity of CT-FFR can mainly be attributed to the error of the TCRI model. It might also explain why the agreement (–0.06 to 0.04) between CT-(Pd/Pa)$_{rest}$ and its invasive value (resting Pd/Pa) outperforms CT-FFR (–0.07 to 0.15), as shown in the result. An early study reported that the gray zone of CT-FFR was 0.70–0.90 (31) and 0.75–0.80 for invasive FFR (32), which showed the gray zone of CT-FFR completely covered that of FFR and was larger than the latter, which supports findings which

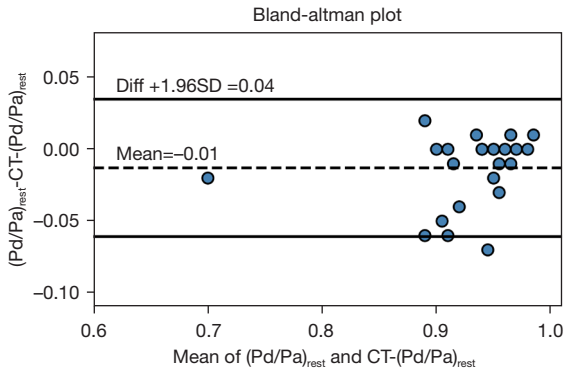

Figure 9 Bland-Altman plot of CT-$(Pd/Pa)_{rest}$ and invasive resting Pd/Pa on a per-vessel basis.

have raised concerns around the accuracy of the gray zone. Cook *et al.* (13) found the accuracy of CT-FFR was only 46.3% within the gray zone, which was dramatically lower than its mean accuracy, suggesting CT-FFR could lose its fidelity in guiding PCI in such a scenario. As mentioned above, in CT-FFR technology, the introduction of the empirical formula of total national resistance index (TCRI) model may limit its diagnostic efficiency in practical clinical application. The concept of CT-Pd/PA is expected to avoid this limitation in identifying functionally relevant coronary artery disease (CAD). As shown in the current study, the gray zone of CT-(Pd/Pa), which was 0.96 to 0.98 when resting Pd/Pa <0.945 was used as a reference, was

Table 3 Per-patient and pre-vessel diagnostic performance of CT-FFR, CT$(Pd/Pa)_{rest}$

	Resting Pd/Pa <0.945 (FFR <0.80 as reference)	CT-FFR <0.80 (FFR <0.80 as reference)	CT-$(Pd/Pa)_{rest}$ <0.94 (Pd/Pa<0.94 as reference)	CT-$(Pd/Pa)_{rest}$ <0.945 (FFR <0.80 as reference)
Accuracy	92	72	88	88
Sensitivity	100	85	80	85
Specificity	83	58	100	91
PPV	87	69	100	92
NPV	100	78	77	83

PPV, positive predictive value; NPV, negative predictive value; CT-FFR, computed tomography angiography-derived fractional flow reserve.

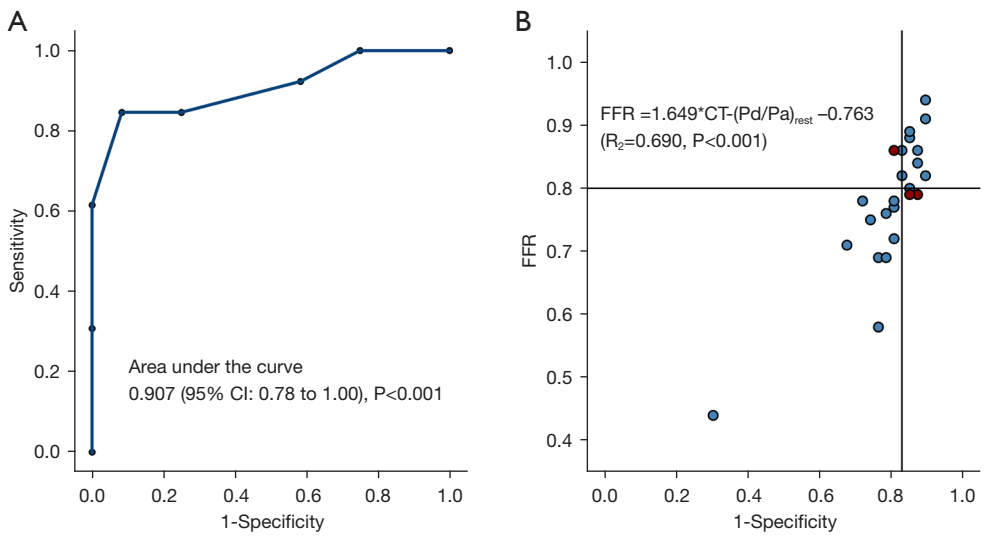

Figure 10 Diagnostic accuracy of resting CT-$(Pd/Pa)_{rest}$ against FFR. (A) Area under the curve (AUC) of CT-$(Pd/Pa)_{rest}$ versus invasive FFR for demonstration of ischemia (FFR <0.80) on a per-vessel basis; (B) Linear correlation for CT-$(Pd/Pa)_{rest}$ and invasive FFR. CT-$(Pd/Pa)_{rest}$ <0.945 and FFR <0.80 were cut-offs for the diagnosis of ischemia. N=25 for per-vessel analysis. FFR, fractional flow reserve.

far smaller than that of CT-FFR when invasive FFR <0.80 was taken as reference. The percentage of misdiagnosis was much lower in the gray zone of CT-$(Pd/Pa)_{rest}$ than CT-FFR, indicating CT-$(Pd/Pa)_{rest}$ may have a better diagnostic performance than CT-FFR in guiding PCI. Our results demonstrate that the discordance between CT-FFR and FFR arises from the physiological discrepancy of the coronary arteries at resting and maximum hyperemia state, and this can be avoided by using CT-$(Pd/Pa)_{rest}$ as a pre-operation diagnosis.

One of the major limitations of this study was its limited number of subjects, and future studies should employ greater patient numbers.

Conclusions

A patient-specific CT-derived resting Pd/Pa method was tested with the purpose of eliminating the main source of error in CT-FFR simulation caused by the simplified TCRI model. Our preliminary results suggest that the CT-derived resting Pd/Pa shows similar or even slightly better diagnostic performance in comparison with CT-FFR. As invasive resting Pd/Pa is being widely adopted in catheter labs, more attention should be given to CT-$(Pd/Pa)_{rest}$ as a potential alternative physiological index for non-invasive stenosis evaluation, in addition to CT-FFR measurement. However, large-scale clinical trials should be conducted to further verify the current findings.

Acknowledgments

Funding: This study was supported by National Natural Science Foundation of China (Grant No. 82070301).

Footnote

Reporting Checklist: The authors have completed the STARD reporting checklist. Available at https://dx.doi.org/10.21037/atm-21-4325

Data Sharing Statement: Available at https://dx.doi.org/10.21037/atm-21-4325

Conflicts of Interest: All authors have completed the ICMJE uniform disclosure form (available at https://dx.doi.org/10.21037/atm-21-4325). Dr. CW and Dr. YM report that they are from Shenzhen Escope Tech Inc. The other authors have no conflicts of interest to declare.

Ethical Statement: The authors are accountable for all aspects of the work in ensuring that questions related to the accuracy or integrity of any part of the work are appropriately investigated and resolved. All procedures performed in this study involving human participants were in accordance with the Declaration of Helsinki (as revised in 2013). The study was approved by Beijing Anzhen Hospital committee board of ethics (No.: 2020091X) and informed consent was taken from all the patients.

References

1. Pijls NH, van Son JA, Kirkeeide RL, et al. Experimental basis of determining maximum coronary, myocardial, and collateral blood flow by pressure measurements for assessing functional stenosis severity before and after percutaneous transluminal coronary angioplasty. Circulation 1993;87:1354-67.
2. van de Hoef TP, Meuwissen M, Escaned J, et al. Fractional flow reserve as a surrogate for inducible myocardial ischaemia. Nat Rev Cardiol 2013;10:439-52.
3. Chamuleau SA, Meuwissen M, van Eck-Smit BL, et al. Fractional flow reserve, absolute and relative coronary blood flow velocity reserve in relation to the results of technetium-99m sestamibi single-photon emission computed tomography in patients with two-vessel coronary artery disease. J Am Coll Cardiol 2001;37:1316-22.
4. Neumann FJ, Sousa-Uva M, Ahlsson A, et al. 2018 ESC/EACTS Guidelines on myocardial revascularization. Eur Heart J 2019;40:87-165.
5. Adjedj J, De Bruyne B, Floré V, et al. Significance of Intermediate Values of Fractional Flow Reserve in Patients With Coronary Artery Disease. Circulation 2016;133:502-8.
6. Echavarría-Pinto M, van de Hoef TP, Garcia-Garcia HM, et al. Diagnostic Accuracy of Baseline Distal-to-Aortic Pressure Ratio to Assess Coronary Stenosis Severity:

A Post-Hoc Analysis of the ADVISE II Study. JACC Cardiovasc Interv 2015;8:834-6.
7. Jeremias A, Maehara A, Généreux P, et al. Multicenter core laboratory comparison of the instantaneous wave-free ratio and resting Pd/Pa with fractional flow reserve: the RESOLVE study. J Am Coll Cardiol 2014;63:1253-61.
8. Lee JM, Park J, Hwang D, et al. Similarity and Difference of Resting Distal to Aortic Coronary Pressure and Instantaneous Wave-Free Ratio. J Am Coll Cardiol 2017;70:2114-23.
9. van Lavieren MA, Piek JJ. Resting Indices of Coronary Lesion Severity: Not Always as Simple as It Seems. Circ Cardiovasc Interv 2016;9:e003747.
10. Maini R, Moscona J, Sidhu G, et al. Pooled diagnostic accuracy of resting distal to aortic coronary pressure referenced to fractional flow reserve: The importance of resting coronary physiology. J Interv Cardiol 2018;31:588-98.
11. Nørgaard BL, Leipsic J, Gaur S, et al. Diagnostic performance of noninvasive fractional flow reserve derived from coronary computed tomography angiography in suspected coronary artery disease: the NXT trial (Analysis of Coronary Blood Flow Using CT Angiography: Next Steps). J Am Coll Cardiol 2014;63:1145-55.
12. Patel MR, Nørgaard BL, Fairbairn TA, et al. 1-Year Impact on Medical Practice and Clinical Outcomes of FFR(CT): The ADVANCE Registry. JACC Cardiovasc Imaging 2020;13:97-105.
13. Cook CM, Petraco R, Shun-Shin MJ, et al. Diagnostic Accuracy of Computed Tomography-Derived Fractional Flow Reserve: A Systematic Review. JAMA Cardiol 2017;2:803-10.
14. Fossan FE, Sturdy J, Müller LO, et al. Uncertainty Quantification and Sensitivity Analysis for Computational FFR Estimation in Stable Coronary Artery Disease. Cardiovasc Eng Technol 2018;9:597-622.
15. Johnson NP, Kirkeeide RL, Gould KL. Is discordance of coronary flow reserve and fractional flow reserve due to methodology or clinically relevant coronary pathophysiology? JACC Cardiovasc Imaging 2012;5:193-202.
16. Sankaran S, Grady L, Taylor CA. Fast Computation of Hemodynamic Sensitivity to Lumen Segmentation Uncertainty. IEEE Trans Med Imaging 2015;34:2562-71.
17. Uzu K, Otake H, Choi G, et al. Lumen boundaries extracted from coronary computed tomography angiography on computed fractional flow reserve (FFRCT): validation with optical coherence tomography. EuroIntervention 2019;14:e1609-18.
18. Taylor CA, Fonte TA, Min JK. Computational fluid dynamics applied to cardiac computed tomography for noninvasive quantification of fractional flow reserve: scientific basis. J Am Coll Cardiol 2013;61:2233-41.
19. Sharma P, Itu L, Zheng X, et al. A framework for personalization of coronary flow computations during rest and hyperemia. Annu Int Conf IEEE Eng Med Biol Soc 2012;2012:6665-8.
20. Müller LO, Fossan FE, Bråten AT, et al. Impact of baseline coronary flow and its distribution on fractional flow reserve prediction. Int J Numer Method Biomed Eng 2019:e3246.
21. Chen YD, Fang WY, Chen JY, et al. Chinese expert consensus on the non-invasive imaging examination pathways of stable coronary artery disease. J Geriatr Cardiol 2018;15:30-40.
22. Leipsic J, Abbara S, Achenbach S, et al. SCCT guidelines for the interpretation and reporting of coronary CT angiography: a report of the Society of Cardiovascular Computed Tomography Guidelines Committee. J Cardiovasc Comput Tomogr 2014;8:342-58.
23. Kirişli HA, Schaap M, Metz CT, et al. Standardized evaluation framework for evaluating coronary artery stenosis detection, stenosis quantification and lumen segmentation algorithms in computed tomography angiography. Med Image Anal 2013;17:859-76.
24. Medrano-Gracia P, Ormiston J, Webster M, et al. A computational atlas of normal coronary artery anatomy. EuroIntervention 2016;12:845-54.
25. Lardo AC, Rahsepar AA, Seo JH, et al. Estimating coronary blood flow using CT transluminal attenuation flow encoding: Formulation, preclinical validation, and clinical feasibility. J Cardiovasc Comput Tomogr 2015;9:559-66.e1.
26. Tang CX, Liu CY, Lu MJ, et al. CT FFR for Ischemia-Specific CAD With a New Computational Fluid Dynamics Algorithm: A Chinese Multicenter Study. JACC Cardiovasc Imaging 2020;13:980-90.
27. Hennigan B, Oldroyd KG, Berry C, et al. Discordance Between Resting and Hyperemic Indices of Coronary Stenosis Severity: The VERIFY 2 Study (A Comparative Study of Resting Coronary Pressure Gradient, Instantaneous Wave-Free Ratio and Fractional Flow Reserve in an Unselected Population Referred for Invasive Angiography). Circ Cardiovasc Interv 2016;9:e004016.
28. De Luca G, Verdoia M, Barbieri L, et al. Resting Pd/Pa and haemodynamic relevance of coronary stenosis as

evaluated by fractional flow reserve. Coron Artery Dis 2018;29:138-44.
29. Härle T, Bojara W, Meyer S, et al. Comparison of instantaneous wave-free ratio (iFR) and fractional flow reserve (FFR)--first real world experience. Int J Cardiol 2015;199:1-7.
30. Chowdhury M, Osborn EA. Physiological Assessment of Coronary Lesions in 2020. Curr Treat Options Cardiovasc Med 2020;22:2.
31. Villines TC. Can CT-derived FFR better inform clinical decision-making and improve outcomes in stable ischaemic heart disease? Eur Heart J 2018;39:3712-4.
32. Escaned J, Echavarría-Pinto M, Garcia-Garcia HM, et al. Prospective Assessment of the Diagnostic Accuracy of Instantaneous Wave-Free Ratio to Assess Coronary Stenosis Relevance: Results of ADVISE II International, Multicenter Study (ADenosine Vasodilator Independent Stenosis Evaluation II). JACC Cardiovasc Interv 2015;8:824-33.

(English Language Editor: B. Draper)

Cite this article as: Li Q, Zhang Y, Wang C, Dong S, Mao Y, Tang Y, Zeng Y. Diagnostic performance of CT-derived resting distal to aortic pressure ratio (resting Pd/Pa) *vs.* CT-derived fractional flow reserve (CT-FFR) in coronary lesion severity assessment. Ann Transl Med 2021;9(17):1390. doi: 10.21037/atm-21-4325

